CHEMISTRY OF MATERIALS

pubs.acs.org/cm

Article

Thermal Atomic Layer Etching of Gallium Oxide Using Sequential Exposures of HF and Various Metal Precursors

Younghee Lee, Nicholas R. Johnson, and Steven M. George*

Cite This: *Chem. Mater.* 2020, 32, 5937−5948

Read Online

ACCESS | Metrics & More | Article Recommendations

ABSTRACT: Gallium oxide (Ga_2O_3) is a transparent semiconducting oxide with a large band gap that has applications for power electronics and optoelectronics. Ga_2O_3 device fabrication requires etching for many processing steps. In this work, the thermal atomic layer etching (ALE) of Ga_2O_3 was performed using hydrofluoric acid (HF) and a wide range of different metal precursors including BCl_3, $AlCl(CH_3)_2$, $Al(CH_3)_3$, $TiCl_4$, and $Ga(N(CH_3)_2)_3$. Because Ga_2O_3 is not a particularly stable oxide, the B-, Al-, or Ti-containing metal precursors can possibly convert the surface of Ga_2O_3 to B_2O_3, Al_2O_3, or TiO_2. These metal precursors can also provide Cl, CH_3, and $N(CH_3)_2$ ligands for ligand-exchange reactions. Consequently, the thermal ALE of Ga_2O_3 can occur via "conversion-etch" or fluorination and ligand-exchange reaction pathways. Using sequential HF and BCl_3 exposures and in situ spectroscopic ellipsometry techniques, Ga_2O_3 etch rates were observed to vary from 0.59 to 1.35 Å/cycle at temperatures from 150 to 200 °C, respectively. The Ga_2O_3 etch rates were also self-limiting versus HF and BCl_3 exposure. The lack of BCl_3 pressure dependence for the etch rates argued against the conversion-etch mechanism and in favor of a fluorination and ligand-exchange reaction pathway. In situ quartz crystal microbalance techniques also revealed that Ga_2O_3 could be etched using sequential exposures of HF and various other metal precursors. Ga_2O_3 etch rates at 250 °C were 1.2, 0.82, 0.85, and 0.23 Å/cycle for $AlCl(CH_3)_2$, $Al(CH_3)_3$, $TiCl_4$, and $Ga(N(CH_3)_2)_3$ as the metal precursors, respectively. The mass changes during the individual exposures of HF and the $AlCl(CH_3)_2$ and $Al(CH_3)_3$ metal precursors argued for a fluorination and ligand-exchange mechanism. The $AlCl(CH_3)_2$ and $Al(CH_3)_3$ exposures may also lead to some conversion of Ga_2O_3 to Al_2O_3. In contrast, the mass changes during the HF and $TiCl_4$ exposures were consistent with the conversion of the surface of Ga_2O_3 to TiO_2 and then the spontaneous removal of the TiO_2 surface layer by HF. Distinctly different behavior was observed during the HF and $Ga(N(CH_3)_2)_3$ exposures. The large mass gain during the $Ga(N(CH_3)_2)_3$ exposures suggested that $Ga(N(CH_3)_2)_3$ can adsorb on the fluorinated Ga_2O_3 surface prior to the ligand-exchange reaction. The wide range of metal precursors that can etch Ga_2O_3 argues that the ability of these precursors to convert Ga_2O_3 or to undergo ligand-exchange reactions provides multiple pathways for effective thermal Ga_2O_3 ALE.

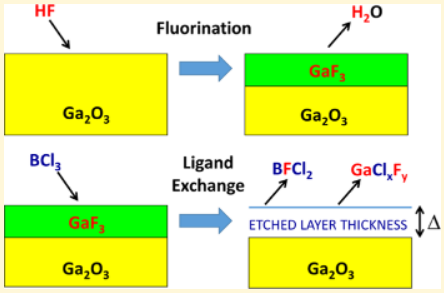

1. INTRODUCTION

Atomic layer etching (ALE) can remove surface material with Ångstrom-level precision using two sequential, self-limiting surface reactions.[1,2] The first reaction usually modifies the surface by halogenation or oxidation. The second reaction is able to remove the modified surface species by producing volatile etching products. Atomic-layer-controlled etching then results from the sequential surface modification and removal reactions.[1,2] Many ALE processes have been developed recently for a variety of materials.

ALE can be accomplished using either plasma ALE or thermal ALE.[2−4] Plasma ALE produces anisotropic etching by employing energetic ions or neutrals to remove the modified surface species by a sputtering process.[2] Plasma Si ALE is the model plasma ALE system that has been demonstrated using halide adsorption and Ar^+ ion exposures.[5−8] A variety of other plasma ALE processes have been developed for SiO_2,[9,10] HfO_2,[11] Al_2O_3,[12] InP,[13] GaN,[14] W,[15] graphene,[16] and polymers.[17]

Thermal atomic layer etching (ALE) produces isotropic etching using thermal reactions for etching.[3,4,18−20] Many different pathways have been documented for thermal ALE.[21] Fluorination and ligand-exchange reactions define the mechanism for the thermal ALE of many metal oxides and metal nitrides.[3,4] Fluorination and ligand-exchange reactions have been utilized for the thermal ALE of Al_2O_3,[4,18−20,22−27] HfO_2,[20,23,25,28] ZrO_2,[20,25] AlN,[29] GaN,[30] and VO_2.[22] Other pathways for thermal ALE employ conversion, oxidation, and halogenation mechanisms.[21] During the conversion mechanism, reactions convert the surface of the initial material to a

Received: January 12, 2020
Revised: June 18, 2020
Published: June 19, 2020

https://dx.doi.org/10.1021/acs.chemmater.0c00131
Chem. Mater. 2020, 32, 5937−5948

new material prior to etching. The conversion mechanism has been utilized for the thermal ALE of ZnO,[31] SiO_2,[32] W,[33] WO_3,[33] Si ALE,[34] and SiN.[35]

Interest in Ga_2O_3 is high because of its possible application in power electronics and optoelectronics.[36−40] In particular, Ga_2O_3 has properties that are favorable for high-power and high-mobility devices.[37,38,40,41] Ga_2O_3 has a high breakdown voltage and large band gap of 4.5−4.9 eV.[37,42] The breakdown voltage of Ga_2O_3 is more than 2 times greater than SiC or GaN allowing for more than triple the power performance.[37] In addition, the saturation electron drift velocity of Ga_2O_3 is estimated to be 2×10^7 cm/s,[43] which is more than double the saturation electron drift velocity of Si.[44]

Ga_2O_3 has already proven itself in a number of device applications. Field-effect transistor (FET) devices have been fabricated based on Ga_2O_3.[42] Vertical Ga_2O_3 FETs were shown to be suitable for high-power and voltage applications.[45,46] Ga_2O_3 FETs were also constructed having stable device performance up to 300 °C with large on/off ratios larger than 10 orders of magnitude.[47] Ga_2O_3 ALD films have also been used as gate dielectrics and have displayed gate leakage 2 orders of magnitude lower than conventional high-electron-mobility transistors (HEMTs).[48]

The etching of Ga_2O_3 is critical to produce Ga_2O_3 devices.[39] Ga_2O_3 can be etched using chlorine-containing plasma chemistries to produce volatile products such as $GaCl_3$.[39] BCl_3 has been used as the reactant gas with both reactive ion etching (RIE) and inductively coupled plasma (ICP) etch conditions.[49] Cl_2 and mixtures of Cl_2/BCl_3 reactant gases have also been successful for the plasma etching of Ga_2O_3.[39,49,50] Although conventional RIE and ICP etching procedures can remove Ga_2O_3, there have been no reported processes for atomic-layer-controlled Ga_2O_3 etching using either plasma or thermal ALE.

This work explores thermal Ga_2O_3 ALE using a variety of different metal precursors including BCl_3, $AlCl(CH_3)_2$ (dimethylaluminum chloride (DMAC)), $Al(CH_3)_3$ (trimethylaluminum (TMA)), $TiCl_4$, and $Ga(N(CH_3)_2)_3$ (tris-dimethylamido-gallium, (TDMAG)). Because Ga_2O_3 does not have a high heat of formation and is not a particularly stable oxide, the mechanism of thermal Ga_2O_3 ALE could occur by conversion reactions or fluorination and ligand-exchange reactions. Conversion reactions occur when the metal precursor can form a more stable oxide on the Ga_2O_3 surface.

Thermochemical calculations indicate that BCl_3, $TiCl_4$, and $Al(CH_3)_3$ could all convert the Ga_2O_3 surface to more stable oxides. The standard free energy changes for these reactions at 200 °C are shown below[51]

$$Ga_2O_3 + 2BCl_3(g) \rightarrow B_2O_3 + 2GaCl_3(g)$$
$$\Delta G°(200\ °C) = -62\ \text{kcal} \quad (1)$$

$$Ga_2O_3 + 1.5TiCl_4(g) \rightarrow 1.5TiO_2 + 2GaCl_3(g)$$
$$\Delta G°(200\ °C) = -23\ \text{kcal} \quad (2)$$

$$Ga_2O_3 + 2Al(CH_3)_3(g) \rightarrow Al_2O_3 + 2Ga(CH_3)_3(g)$$
$$\Delta G°(200\ °C) = -173\ \text{kcal} \quad (3)$$

Following these conversion reactions, the B_2O_3 and TiO_2 surface layers could then be spontaneously removed by hydrofluoric acid (HF) as demonstrated previously.[33,52] The Al_2O_3 layer could also be fluorinated to produce AlF_3 or AlO_xF_y.[26,53] This fluoride layer could then be removed by ligand-exchange reactions.[3,4,20,23,24]

Alternatively, thermal Ga_2O_3 ALE could occur via the fluorination and ligand-exchange mechanism. HF could fluorinate the Ga_2O_3 surface to GaF_3 because this reaction is favorable as predicted by a negative standard free energy change[51]

$$Ga_2O_3 + 6HF(g) \rightarrow 2GaF_3 + 3H_2O(g)$$
$$\Delta G°(200\ °C) = -41\ \text{kcal} \quad (4)$$

After the GaF_3 layer is formed, GaF_3 could be etched by ligand-exchange reactions with BCl_3 because these reactions are also favorable. For example, ligand-exchange between GaF_3 and BCl_3 leading to BF_3 and $GaCl_3$ reaction products has a negative standard free energy change[51]

$$GaF_3 + BCl_3(g) \rightarrow BF_3(g) + GaCl_3(g)$$
$$\Delta G°(200°C) = -19\ \text{kcal} \quad (5)$$

In contrast, the GaF_3 layer may not be easily removed by $TiCl_4$ because this ligand-exchange reaction has a positive standard free energy change[51]

$$GaF_3 + 3/4TiCl_4(g) \rightarrow 3/4TiF_4(g) + GaCl_3(g)$$
$$\Delta G°(200\ °C) = +14\ \text{kcal} \quad (6)$$

On the other hand, the GaF_3 layer should be removed by $Al(CH_3)_3$ as anticipated from previous mass spectrometric studies of AlF_3 etching by $Al(CH_3)_3$[54]

$$GaF_3 + 2Al(CH_3)_3(g) \rightarrow GaF(CH_3)_2(g) + 2AlF(CH_3)_2(g) \quad (7)$$

$AlF(CH_3)_2$ has been observed as an etch product during Al_2O_3 ALE using HF and $Al(CH_3)_3$ as the reactants.[54]

The ability of Ga_2O_3 to undergo thermal ALE by either conversion reactions or fluorination and ligand-exchange reactions may lead to efficient thermal ALE. This work will assess whether thermal Ga_2O_3 ALE can occur via the "conversion-etch" or the fluorination and ligand-exchange mechanism. The BCl_3, $AlCl(CH_3)_2$, $Al(CH_3)_3$, $TiCl_4$, and $Ga(N(CH_3)_2)_3$ metal precursors can provide Cl, CH_3, and $N(CH_3)_2$ ligands. These metal precursors may be able to etch Ga_2O_3 if the products from the conversion and ligand-exchange reactions are stable and volatile. Quantifying the differences between the various metal precursors will help to develop an understanding of the underlying conversion or ligand-exchange reactions.

2. EXPERIMENTAL SECTION

2.1. In Situ Measurements of Ga_2O_3 ALE Using BCl_3. For the studies of Ga_2O_3 ALE using BCl_3, Ga_2O_3 samples were deposited on a thermal SiO_2 layer with a thickness of 5000 Å on a silicon coupon. Ga_2O_3 films were grown using atomic layer deposition (ALD) techniques using sequential trimethylgallium (Sigma-Aldrich 99.9999%) and O_2 (Airgas UHP) plasma exposures at 200 °C.[55] The trimethylgallium (TMG) was dosed statically for 5 s at a pressure of 120 mTorr. O_2 was introduced into the chamber for 25 s. The O_2 plasma at a power of 400 W was ignited after 5 s and the O_2 plasma exposure occurred for 20 s.

An inductively coupled plasma (ICP) source created the O_2 plasma that produced the oxygen radicals for Ga_2O_3 ALD. The ICP source was a helical copper coil wrapped around a quartz tube with an inner diameter of 6 cm and a length of 25 cm. A 50 Ω impedance matching

https://dx.doi.org/10.1021/acs.chemmater.0c00131
Chem. Mater. 2020, 32, 5937−5948

network (Navigator Digital Matching Network, Advanced Energy) and a 13.56 MHz RF generation (Paramount RF Power Supply, Advanced Energy) were used together to generate the plasma. The reaction chamber has been described previously.[29,33,56] The chamber was pumped with a mechanical pump (Pascal 2015 SD, Alcatel Adixen). The chamber walls of the reactor were heated to 170 °C for all experiments.

BCl_3 (Synquest Laboratories, 99.9%) and HF-Pyridine (Sigma-Aldrich 70 wt. % HF) were used as the reactants for etching. Each reactant was dosed separately and statically into the chamber with a background Argon pressure of 1.2 Torr. After the BCl_3 exposure, the chamber was purged for 60 s. After the HF exposure, the chamber was purged for 70 s. Each reactant was purged with flowing Argon at a pressure of 1.2 Torr. A capacitance manometer was used for pressure measurements.

HF derived from the HF-pyridine solution avoids the difficulty of handling HF from anhydrous HF gas cylinders. The vapor pressure of HF above the HF-pyridine solution is 90−100 Torr at room temperature.[57] Unreacted HF exiting the reactor was captured first by an activated alumina trap (Visi-Trap, LACO Technologies) located on the inlet of the mechanical pump. The remaining HF was neutralized by bubbling the gas exhaust stream from the mechanical pump through a calcium oxide solution. This calcium oxide solution was located immediately after the mechanical pump.

The Ga_2O_3 etching was analyzed by in situ spectroscopic ellipsometry (SE) using a spectroscopic ellipsometer (M-2000D, J.A. Woollam). The incident angle for all SE experiments was 70°. The ellipsometer had a spectral range from 239.2 to 1687.2 nm. The Ga_2O_3 films were analyzed using commercial software (CompleteEASE, J.A. Woollam). A Cauchy dispersion model was used for film thickness measurements because Ga_2O_5 has a large band gap of ∼4.5−4.9 eV. All parameters of the Cauchy model were varied for accurate film measurements. The index of refraction for the Ga_2O_3 films remained ∼1.85−1.86 throughout etching.

2.2. In Situ Measurements of Ga_2O_3 ALE Using Various Other Metal Precursors. For the Ga_2O_3 ALE studies using $AlCl(CH_3)_2$, $Al(CH_3)_3$, $TiCl_4$, and $Ga(N(CH_3)_2)_3$, the ALD and ALE reactions were conducted in a viscous flow reactor described previously.[58] The stainless steel reactor tube was isothermally heated by ceramic fiber heaters (275 and 550 W, Watlow). The temperature was maintained by a proportional-integral-derivative (PID) temperature controller (2604, Eurotherm). The pressure was monitored by a capacitance manometer (Baratron 121A, MKS). A constant flow of 150 sccm of ultra-high-purity (UHP) N_2 gas was supplied by mass flow controllers (Type 1179A, MKS) into the reactor. This N_2 gas flow produced a pressure of ∼1 Torr in the reactor that was pumped using a mechanical pump (Pascal 2015 SD, Alcatel Adixen).

A film deposition monitor (Maxtek TM-400, Inficon) measured the mass changes during in situ QCM measurements.[58] The quartz crystal (gold coated and polished, 6 MHz crystal, Colnatec) was placed in a bakeable single sensor head (BSH-150, Inficon) and sealed with high-temperature epoxy (Epo-Tek H21D, Epoxy Technology). Deposition on the backside of the QCM sensor was prevented by flowing an additional 20 sccm of N_2 through the QCM housing.[58] This additional N_2 was supplied using a bellows-sealed metering valve (SS-4BMG, Swagelok).

Thermal Ga_2O_3 ALD was conducted using sequential exposures of tris(dimethylamido)gallium (TDMAG, 98%, Sigma-Aldrich) and deionized H_2O at 200 °C.[59] Thermal Ga_2O_3 ALD was utilized for the QCM measurements because the viscous flow reactor does not contain a plasma source. The TDMAG precursor was maintained at 105 °C to yield pressure transients of 5−10 mTorr. The reaction sequence was 1-30-1-30. This reaction sequence designates an exposure of TDMAG precursor for 1 s, a N_2 purge for 30 s, an H_2O exposure for 1 s, and a N_2 purge for 30 s. The Ga_2O_3 ALD films were deposited on Al_2O_3 ALD films. The growth of the Al_2O_3 ALD films was conducted using trimethylaluminum (TMA) (97%, Sigma-Aldrich) and H_2O.

The fluorination reaction employed HF vapor derived from an HF-pyridine solution (70 wt % HF, Sigma-Aldrich).[23,60,61] The HF-pyridine solution was transferred to a gold-plated, stainless steel bubbler in a dry N_2-filled glovebag and maintained at room temperature. No measurable pyridine vapor was detected by mass spectrometry.[60] The HF pressure transients were adjusted to ∼80 mTorr using a metering valve.

The metal precursors were trimethylaluminum (TMA, 97%, Sigma-Aldrich), dimethylaluminum chloride (DMAC, 97%, Sigma-Aldrich), TDMAG, and titanium tetrachloride ($TiCl_4$, 99.0% Fluka). The TMA, DMAC, and $TiCl_4$ reactants were held at room temperature. The TMA and DMAC pressure transients were adjusted to ∼40 mTorr using metering valves. The TDMAG precursor was maintained at 105 °C to yield pressure transients of 5−10 mTorr. Titanium tetrachloride ($TiCl_4$, 99.0% Fluka) was transferred to a glass bubbler in a dry N_2-filled glovebag and maintained at room temperature. The $TiCl_4$ transients were adjusted to 120 mTorr using a metering valve.

2.3. Ex Situ Measurements of Ga_2O_3 ALE. For the ex situ measurements of Ga_2O_3 ALE, Ga_2O_3 films were grown on boron-doped Si (100) wafers (p type, Silicon Valley Microelectronics). The Si wafer was cleaved into coupons with dimensions of 2.5 cm by 2.5 cm. Five Si coupons could be coated simultaneously during Ga_2O_3 ALD using TDMAG and H_2O. The ALE reactions were performed using a reaction sequence designated as 2-30-1-30. This reaction sequence consists of an exposure of metal precursor for 2 s, a N_2 purge for 30 s, an HF exposure derived from the HF-pyridine solution for 1 s, and a N_2 purge for 30 s.

The thickness of the Ga_2O_3 films on the Si(100) coupons was measured by ex situ SE measurements. A spectroscopic ellipsometer (M-2000, J. A. Woollam) measured Ψ and Δ at 240−1700 nm with an incidence angle of 75°. The analysis software (CompleteEASE, J. A. Woollam) fitted Ψ and Δ to obtain the thickness and refractive index of the film. A Tauc−Lorentz model was used to determine the thickness of the Ga_2O_3 films.

The X-ray reflectivity (XRR) measurements were performed with a high resolution X-ray diffractometer (Bede D1, Jordan Valley Semiconductors) using Cu Kα (λ = 1.540 Å) radiation. The X-ray tube filament voltage and current were 40 kV and 35 mA, respectively. XRR scans ranged from 300 to 6000 arcsec and were recorded with a 10 arcsec step size. The analysis software (Bede REFS, Jordan Valley Semiconductors) determined film thickness by fitting of the XRR scans.

X-ray photoelectron spectroscopy (XPS) measured the film composition using a commercial XPS instrument (PHI 5600, RBD Instruments). A monochromatic Al Kα X-ray source (1486.6 eV) was used to collect survey scans with a pass energy of 93.9 eV and a step size of 0.400 eV. The Auger Scan software package (Auger Scan, RBD Instruments) was employed to collect the data. Casa XPS software (Casa XPS, Casa Software) determined the surface concentrations.

3. RESULTS AND DISCUSSION

3.1. In Situ Measurements of Ga_2O_3 ALE Using BCl_3. Ga_2O_3 ALD film growth as measured by in situ SE studies at 200 °C is shown in Figure 1. The Ga_2O_3 ALD was performed using sequential trimethylgallium (TMG) and O_2 plasma exposures. This Ga_2O_3 ALD process is known to produce amorphous Ga_2O_3 films with no carbon in the bulk of the film.[55] Figure 1 indicates that the Ga_2O_3 growth rate is linear with a growth rate of 0.75 Å/cycle. This growth rate is slightly higher than the earlier reported growth rate of 0.53 Å/cycle using TMG and O_2 plasma.[55] Ga_2O_3 films had an index of refraction of ∼1.85−1.87 measured using SE. This index of refraction is close to the index of refraction of 1.89 for β-Ga_2O_3.[62]

Figure 2 shows the Ga_2O_3 thickness change for a Ga_2O_3 film versus number of ALE cycles at 200 °C. The HF and BCl_3 exposure sequence was defined by a 0.75 s static dose of HF at 400 mTorr and an 8 s static dose of BCl_3 at 500 mTorr. The purge times were 70 s after the HF exposure and 60 s after the

https://dx.doi.org/10.1021/acs.chemmater.0c00131
Chem. Mater. 2020, 32, 5937−5948

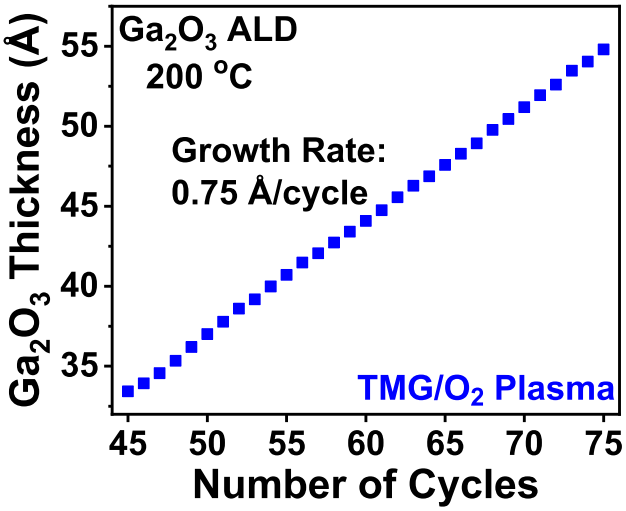

Figure 1. Ga_2O_3 film thickness versus number of cycles of Ga_2O_3 ALD using TMG and O_2 plasma as the reactants at 200 °C. Ga_2O_3 growth rate is 0.75 Å/cycle.

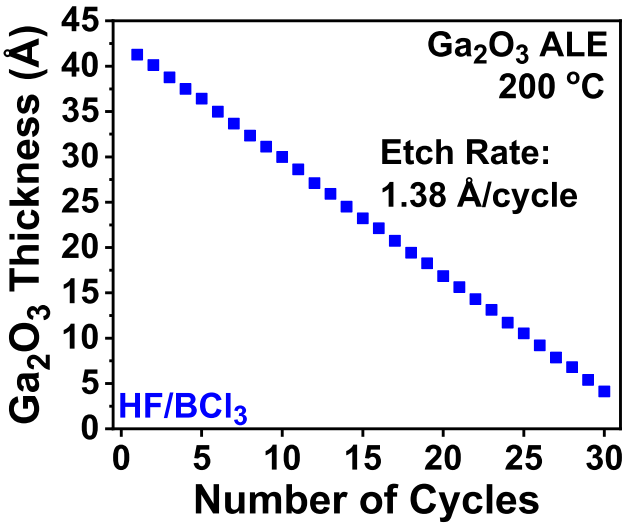

Figure 2. Ga_2O_3 film thickness versus number of cycles of Ga_2O_3 ALE using HF and BCl_3 as the reactants at 200 °C. Ga_2O_3 etch rate is 1.38 Å/cycle.

BCl_3 exposure. The Ga_2O_3 etching is linear with an etch rate of 1.38 Å/cycle. The etch rate at 200 °C under these conditions varied from 1.34 to 1.44 Å/cycle for individual experiments.

The self-limiting behavior for Ga_2O_3 ALE was investigated using HF and BCl_3 as the reactants. The self-limiting behavior for the HF reaction is shown in Figure 3a. BCl_3 was held constant at 500 mTorr statically for 8 s. HF pressure was varied from 120 to 750 mTorr and held statically for 0.75 s. The purge times were again 70 s after the HF exposure and 60 s after the BCl_3 exposure. Progressively higher HF pressures result in higher etch rates until reaching an HF pressure of 300 mTorr. The etch rate is constant at 1.4−1.5 Å/cycle for HF pressures > 300 mTorr.

The fast increase in the etch rate followed by a slow increase prior to reaching self-limiting conditions is similar to the effect of HF pressure on Al_2O_3 ALE using HF and TMA.[26] This behavior is explained by the fluoride layer forming a diffusion barrier on the surface that makes subsequent fluorination more

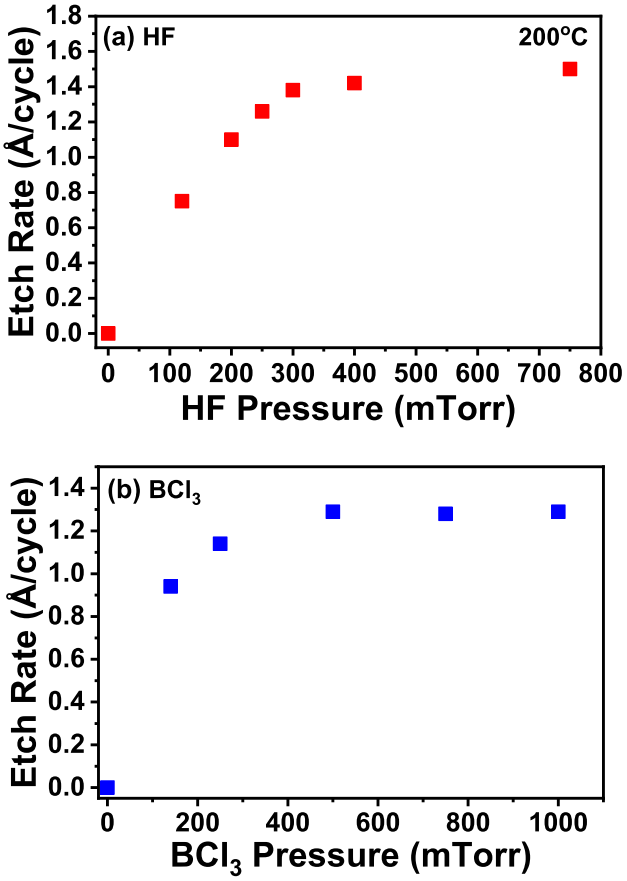

Figure 3. (a) Etch rate for Ga_2O_3 versus HF pressure for 0.75 s. BCl_3 pressure was held statically at 500 mTorr for 8 s. (b) Etch rate for Ga_2O_3 versus BCl_3 pressure for 8 s. HF pressure was held statically at 120 mTorr for 0.75 s.

difficult. The mathematics of surface modification limited by a diffusion barrier has been expressed earlier using the Deal−Grove model.[63] This model was originally developed to explain Si oxidation.[63]

Figure 3b shows the change in the etch rate for Ga_2O_3 versus BCl_3 pressure. BCl_3 pressures were varied from 140 to 1000 mTorr with constant static exposure times of 8 s. The HF was exposed at a pressure of 120 mTorr for 0.75 s. The etch rate increases at higher BCl_3 pressures. No noticeable increase in the etch rate is observed at BCl_3 pressures > 500 mTorr. The BCl_3 reaction for Ga_2O_3 ALE is self-limiting at an etch rate of 1.3 Å/cycle.

The self-limiting nature of the BCl_3 reaction in Figure 3b does not argue for a conversion reaction. If BCl_3 was converting the surface of Ga_2O_3 to B_2O_3, then higher BCl_3 pressures would have been expected to produce thicker B_2O_3 layers in accordance with the Deal−Grove model.[63] The spontaneous etching of the thicker B_2O_3 layers by HF exposure would then lead to higher Ga_2O_3 etching rates.

In comparison, previous studies of GaN ALE using XeF_2 and BCl_3 as the reactants have observed little dependence of the GaN etch rate on BCl_3 pressure.[30] Previous studies of WO_3 ALE using HF and BCl_3 as the reactants have also observed self-limiting WO_3 etch rates after larger BCl_3 exposures.[33] These results could be explained if the diffusion barrier formed during the possible conversion reaction severely limits the conversion. Alternatively, the results could be consistent with

https://dx.doi.org/10.1021/acs.chemmater.0c00131
Chem. Mater. 2020, 32, 5937−5948

an etching mechanism based on fluorination and ligand-exchange reactions. Decisive evidence for either the conversion-etch or fluorination and ligand-exchange pathway is not always available. The etching process may also be a mixture of some surface conversion and some ligand-exchange. Additional mass spectrometric analysis of the volatile reaction products would be useful to confirm the etching mechanism.

Ga_2O_3 ALE was conducted at various temperatures for 30 ALE cycles as shown in Figure 4. The reaction conditions were

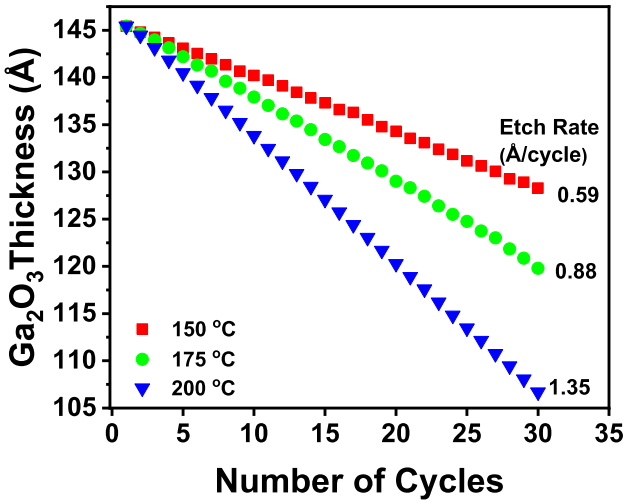

Figure 4. Ga_2O_3 film thickness versus number of cycles of Ga_2O_3 ALE at 150, 175, and 200 °C using HF and BCl_3 as the reactants.

defined by a static dose of BCl_3 for 8 s at 500 mTorr and a static dose of HF for 0.75 s at 400 mTorr. The purge times were 70 s after the HF exposure and 60 s after the BCl_3 exposure. All Ga_2O_3 thicknesses were offset to a thickness of 145 Å to show variation in etching at 150, 175, and 200 °C. The Ga_2O_3 etch rates at 150, 175, and 200 were 0.59, 0.88, and 1.35 Å/cycle, respectively. The Ga_2O_3 ALE is thermally activated as expected for a thermal process. The increase in etch rate may be attributed to larger removal of the GaF_3 layer during the ligand-exchange reactions at higher temperatures.[20,24]

3.2. In Situ Measurements of Ga_2O_3 ALE Using Various Other Metal Precursors. Ga_2O_3 ALD film growth as measured by in situ QCM studies at 200 °C is displayed in Figure 5. The Ga_2O_3 ALD was performed using sequential TDMAG and H_2O exposures. This Ga_2O_3 ALD process produces amorphous Ga_2O_3 films with low-impurity content.[59] The mass change versus time in Figure 5 is linear during 100 Ga_2O_3 ALD cycles using the reaction sequence of 1-30-1-30. The Ga_2O_3 ALD reaction yielded a mass gain per cycle (MGPC) of MGPC = 34 ng/(cm^2 cycle). This MGPC is equivalent to a growth rate of 0.70 Å/cycle at 200 °C based on the Ga_2O_3 ALD film density of 4.8 g/cm^3 measured by X-ray reflectivity (XRR) analysis. This result is comparable with the previous Ga_2O_3 ALD studies using TDMAG and H_2O, where the growth rate was 1.0 Å/cycle at 200 °C.[59] The Ga_2O_3 ALD reactions were also self-limiting. In addition, XPS measurements determined that there were no carbon or nitrogen impurities in the Ga_2O_3 ALD films at levels above the XPS detection limit.

Figure 6 shows Ga_2O_3 ALE performed by HF and TMA exposures with an exposure sequence of 1-30-2-30 monitored

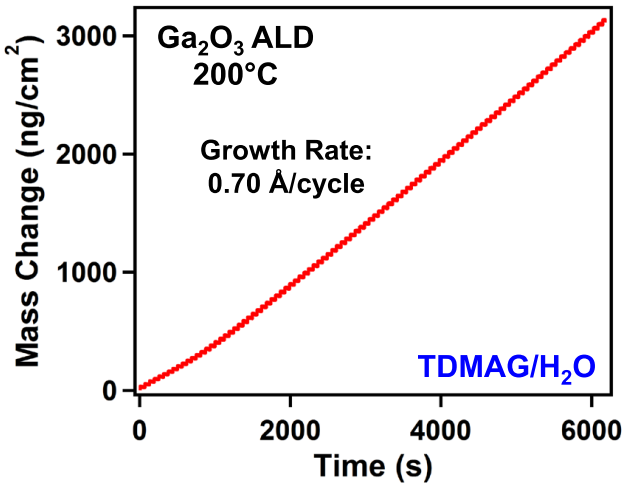

Figure 5. Mass change versus time during 100 Ga_2O_3 ALD cycles with TDMAG and H_2O as the reactants on Al_2O_3 at 200 °C.

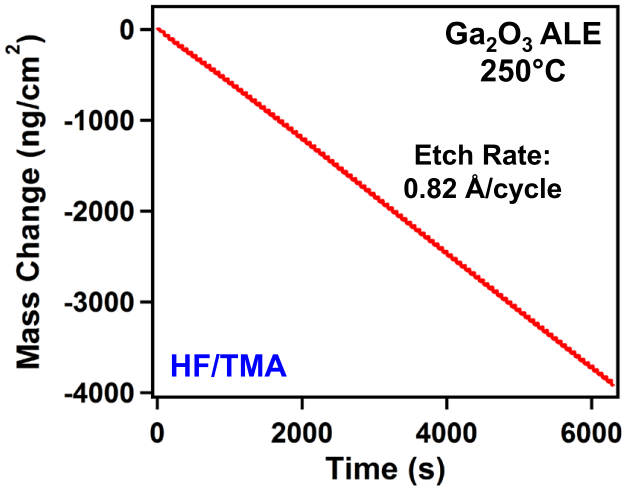

Figure 6. Mass change versus time during 100 Ga_2O_3 ALE cycles with HF and TMA as the reactants at 250 °C.

by in situ QCM at 250 °C. The mass change versus time is displayed during 100 Ga_2O_3 ALE cycles. The initial Ga_2O_3 film on the QCM crystal was grown at 200 °C as shown in Figure 5 to avoid chemical vapor deposition (CVD) reactions occurring at >225 °C. The temperature of the reactor was then elevated to 250 °C for the in situ Ga_2O_3 ALE studies. This procedure avoided breaking vacuum and possible surface contamination of the Ga_2O_3 film upon atmospheric exposure.

Figure 6 reveals that the etching of the Ga_2O_3 film occurs linearly versus HF and TMA sequential exposures. The etch rate from the slope is consistent with a mass change per cycle (MCPC) of MCPC = −39.5 ng/(cm^2 cycle). This etch rate is equivalent to an etch rate of 0.82 Å/cycle. In comparison, this etch rate of 0.82 Å/cycle for Ga_2O_3 is much higher than the etch rate of 0.14 Å/cycle for Al_2O_3 ALE by HF and TMA at 250 °C.[24]

Figure 7 shows an enlargement of the mass changes versus time for three sequential HF and TMA exposures during Ga_2O_3 ALE in the steady-state, linear etching regime shown in Figure 6. The TMA exposures coincide with the mass losses. These mass losses are consistent with either TMA producing volatile etch products by a ligand-exchange reaction or TMA

https://dx.doi.org/10.1021/acs.chemmater.0c00131
Chem. Mater. 2020, 32, 5937−5948

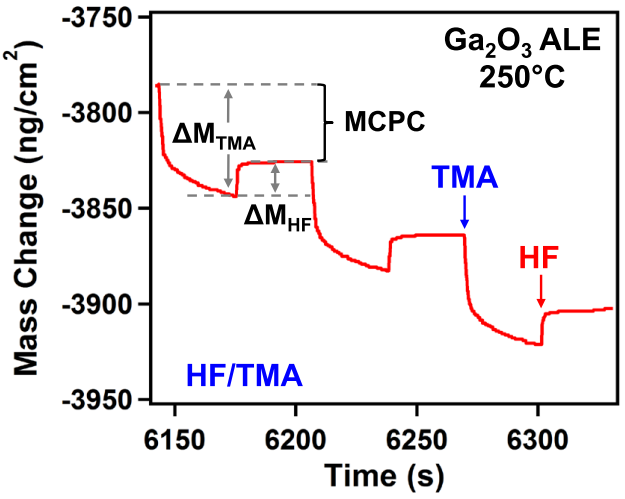

Figure 7. Enlargement of mass change versus time for three sequential HF and TMA exposures during Ga_2O_3 ALE in the steady-state, linear etching regime shown in Figure 6.

converting the surface of Ga_2O_3 to Al_2O_3. The conversion reaction $Ga_2O_3 + 2Al(CH_3)_3(g) \rightarrow Al_2O_3 + 2Ga(CH_3)_3(g)$ would produce a mass loss of 85.5 g/mol.

The subsequent HF exposure in Figure 7 produces a mass gain. This mass gain is expected from fluorination according to $Ga_2O_3 + 6HF(g) \rightarrow 2GaF_3 + 3H_2O(g)$ or $Al_2O_3 + 6HF(g) \rightarrow 2AlF_3 + 3H_2O(g)$. Both of these fluorination reactions have a mass gain of 66.0 g/mol. If the $Al_2O_3 + 6HF(g) \rightarrow 2AlF_3 + 3H_2O(g)$ reaction occurs during the HF exposure, then the subsequent TMA exposure would need to perform a ligand-exchange reaction with the AlF_3 layer prior to the conversion of Ga_2O_3 to Al_2O_3.

The TMA ligand-exchange reaction would first remove the AlF_3 layer. Subsequently, the TMA would continue and perform a conversion reaction to convert Ga_2O_3 to Al_2O_3. A similar dual role of TMA to both remove the AlF_3 layer and convert the underlying oxide layer is believed to be occurring during thermal SiO_2 ALE and ZnO ALE using TMA and HF.[31,32] Consequently, the QCM results could be consistent with both conversion reactions and fluorination and ligand-exchange reactions during thermal Ga_2O_3 ALE using HF and TMA.

Figure 8a shows the mass change after the TMA exposure (ΔM_{TMA}), the mass change after the HF exposure (ΔM_{HF}), and the mass change per cycle (MCPC) versus number of ALE cycles at 250 °C. TMA removes mass with a mass change of $\Delta M_{TMA} = -57.4$ ng/(cm^2 cycle). HF exposures show a mass gain of $\Delta M_{HF} = +17.9$ ng/(cm^2 cycle). The overall mass change per cycle is MCPC = −39.5 ng/(cm^2 cycle). Figure 8b shows the ΔM_{TMA}/MCPC ratio versus number of ALE cycles. The constant ratio of ΔM_{TMA}/MCPC = 1.45 indicates that the surface chemistry does not change during the ALE cycles.

Additional studies showed that HF exposures on a fresh initial Ga_2O_3 ALD surface have a mass change of $\Delta M_{HF} = 19$ ng/cm^2 at 200 °C. Given the stoichiometry of the $Ga_2O_3 + 6HF(g) \rightarrow 2GaF_3 + 3H_2O(g)$ reaction, this mass gain corresponds to the fluorination of 54.3 ng/cm^2 of Ga_2O_3 to 73.3 ng/cm^2 of the GaF_3 layer. Based on the density of 4.8 g/cm^3 for Ga_2O_3, the mass of 54.3 ng/cm^2 for Ga_2O_3 is equivalent to a Ga_2O_3 thickness of 1.1 Å. Similarly, based on the density of 4.5 g/cm^3 for GaF_3, the mass of 73.3 ng/cm^2 for

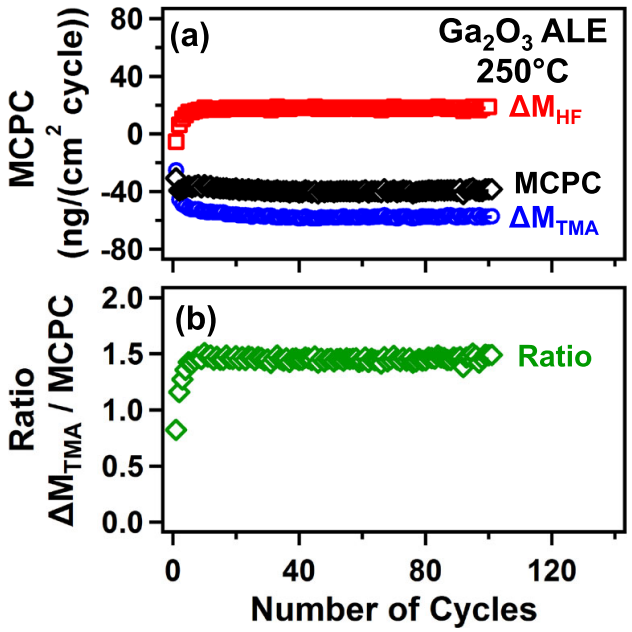

Figure 8. (a) Mass change after TMA exposure (ΔM_{TMA}), mass change after HF exposure (ΔM_{HF}), and mass change per cycle (MCPC) versus number of Ga_2O_3 ALE cycles at 250 °C. (b) ΔM_{TMA}/MCPC ratio versus number of Ga_2O_3 ALE cycles.

GaF_3 is equivalent to a GaF_3 thickness of 1.6 Å. In comparison, earlier studies of the fluorination of initial Al_2O_3 ALD surfaces were consistent with an Al_2O_3 thickness of 1.7 Å fluorinated by HF to produce an AlF_3 thickness of 3.0 Å.[24]

Figures 9−11 show in situ QCM measurements at 250 °C during Ga_2O_3 ALE using HF and three different metal precursors. The results for DMAC, $TiCl_4$, and TDMAG are shown in Figures 9−11, respectively. Similar to the previous experiments using HF and TMA as the reactants, the initial Ga_2O_3 ALD films were first grown on Al_2O_3 ALD films at 200 °C, and then the reaction temperature was increased to 250 °C for the Ga_2O_3 ALE. Mass changes versus time during 20 Ga_2O_3 ALE cycles were recorded using HF exposures with a duration of 1 s and metal precursor exposures with a duration of 2 s.

Figure 9a shows 20 Ga_2O_3 ALE reactions using sequential exposures of HF and DMAC with a reaction sequence of 1-30-2-30. Linear etching was observed with MCPC = −56.9 ng/(cm^2 cycle) at 250 °C. This MCPC is equivalent to an etch rate of 1.2 Å/cycle. This etch rate using HF and DMAC is higher than the etch rate using HF and TMA. DMAC can provide both CH_3 and Cl ligands during the ligand-exchange reaction. Having both CH_3 and Cl ligands may increase the probability of the ligand-exchange reaction.

Figure 9b shows an enlargement of the mass changes versus time for three sequential HF and DMAC exposures during Ga_2O_3 ALE in the steady-state, linear etching regime shown in Figure 9a. The pattern of mass changes during the HF and DMAC exposures is similar to the pattern of mass changes observed during the HF and TMA exposures observed in Figure 7. This similar behavior argues for a fluorination and ligand-exchange mechanism for HF and DMAC. In addition, there could be some conversion of Ga_2O_3 to Al_2O_3 during the DMAC exposure. The mass change during the HF exposure is $\Delta M_{HF} = 17.9$ ng/(cm^2 cycle). The mass change during the DMAC exposure is $\Delta M_{DMAC} = -71.4$ ng/(cm^2 cycle).

https://dx.doi.org/10.1021/acs.chemmater.0c00131
Chem. Mater. 2020, 32, 5937−5948

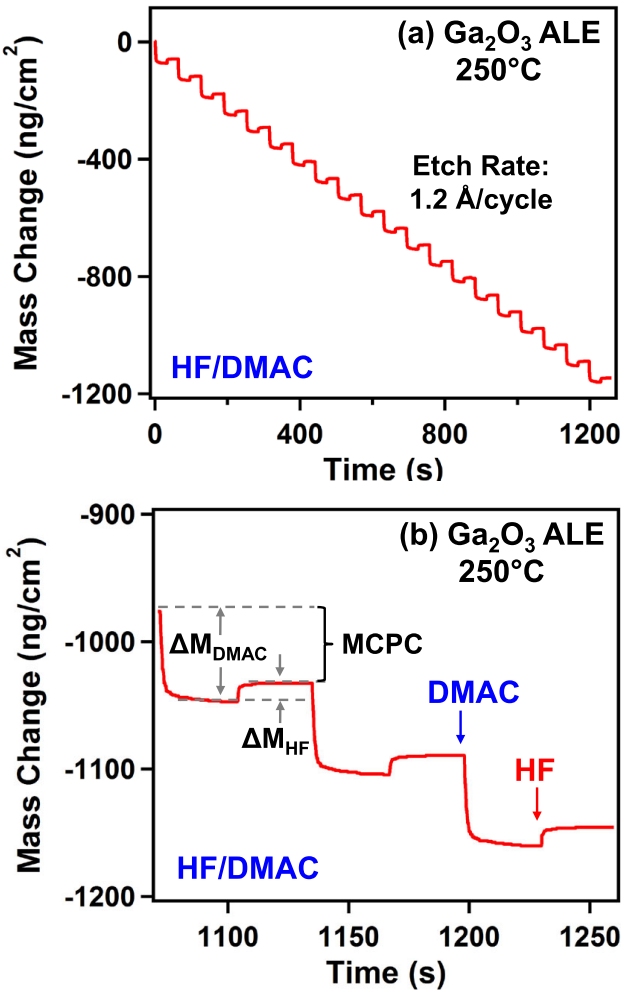

Figure 9. (a) Mass change versus time during 20 Ga_2O_3 ALE cycles with HF and DMAC as the reactants on Ga_2O_3 at 250 °C. (b) Enlargement of mass change versus time for three sequential HF and DMAC exposures during Ga_2O_3 ALE in the steady-state, linear etching regime shown in (a).

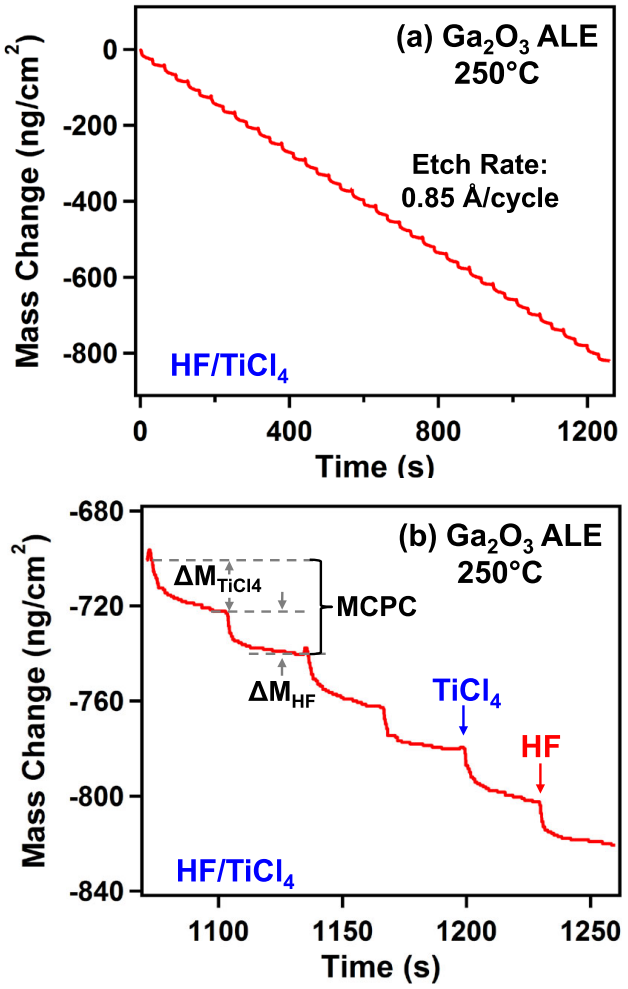

Figure 10. (a) Mass change versus time during 20 Ga_2O_3 ALE cycles with HF and $TiCl_4$ as the reactants on Ga_2O_3 at 250 °C. (b) Enlargement of mass change versus time for three sequential HF and $TiCl_4$ exposures during Ga_2O_3 ALE in the steady-state, linear etching regime shown in (a).

Figure 10a shows Ga_2O_3 ALE performed by 20 sequential HF and $TiCl_4$ exposures with a reaction sequence of 1-30-2-30 at 250 °C. The mass change versus number of ALE cycles yields a mass change per cycle of MCPC = −40.6 ng/(cm^2 cycle). This MCPC corresponds to an etch rate of 0.85 Å/cycle.

Figure 10b shows an enlargement of the mass changes versus time for three sequential HF and $TiCl_4$ exposures during Ga_2O_3 ALE in the steady-state, linear etching regime shown in Figure 10a. The pattern of mass changes in Figure 10b is different than the pattern of mass changes observed for HF and TMA in Figure 7 or HF and DMAC in Figure 9b. The mass changes during the metal precursors are similar. The TMA, DMAC, and $TiCl_4$ metal precursors all produce a mass loss via ligand-exchange or conversion reactions. For example, the mass change during the $TiCl_4$ exposure in Figure 10b is ΔM_{TiCl_4} = −22.9 ng/(cm^2 cycle).

In contrast, the mass change during the HF exposure in Figure 10b is distinctly different than the mass change during the HF exposures in Figures 7 and 9b. The HF exposure in Figure 10b produces a mass loss as opposed to the mass gains observed in Figures 7 and 9b. The mass change during the HF exposure in Figure 10b is ΔM_{HF} = −17.7 ng/(cm^2 cycle). These results suggest that $TiCl_4$ converts the surface of Ga_2O_3 to TiO_2. Then, HF spontaneously etches the TiO_2 layer and produces the pronounced mass loss. The spontaneous etching of TiO_2 by HF was observed earlier during studies of TiN ALE.[52]

The mass changes in Figure 10b cannot easily be interpreted using a fluorination and ligand-exchange mechanism. The fluorination of Ga_2O_3 to GaF_3 should produce a mass gain. However, Figure 10b shows a mass loss during the HF exposure. If HF fluorinates Ga_2O_3 to GaF_3, then $TiCl_4$ would need to remove GaF_3 by a ligand-exchange reaction. However, this ligand-exchange reaction is not thermochemically favorable. Assuming ligand-exchange reactions that transform GaF_3 to $GaCl_3$, the standard free energy change is positive[51]

$$GaF_3 + 3/4TiCl_4(g) \rightarrow GaCl_3(g) + 3/4TiF_4(g)$$
$$\Delta G°(200\ °C) = +13.9\ \text{kcal} \quad (8)$$

In contrast, the conversion of Ga_2O_3 to TiO_2 by $TiCl_4$ is thermochemically favorable as shown in eq 2. The spontaneous

https://dx.doi.org/10.1021/acs.chemmater.0c00131
Chem. Mater. 2020, 32, 5937−5948

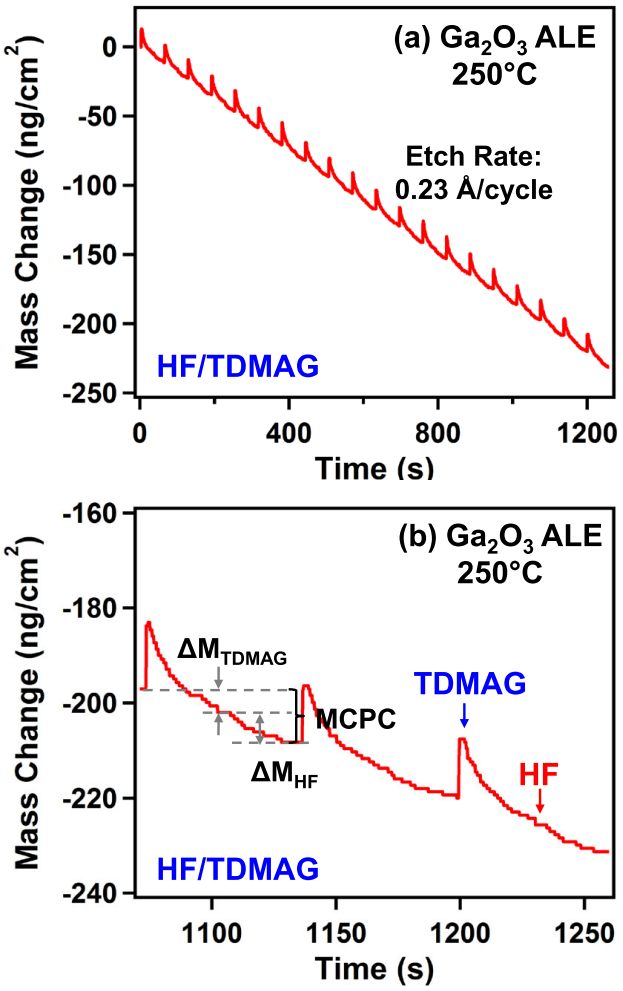

Figure 11. (a) Mass change versus time during 20 Ga_2O_3 ALE cycles with HF and TDMAG as the reactants on Ga_2O_3 at 250 °C. (b) Enlargement of mass change versus time for three sequential HF and TDMAB exposures during Ga_2O_3 ALE in the steady-state, linear etching regime shown in (a).

etching of TiO_2 by HF has also been confirmed by recent studies.[52]

An alternative explanation for the mass changes in Figure 10b is that HF fluorinates Ga_2O_3 and produces a mass gain. However, F/Cl exchange also yields a larger mass loss that produces a net mass loss during the HF exposure. This fluorination would then need to be followed by a thermochemically unfavorable ligand-exchange reaction as given by eq 8. The results in Figure 10b are more in agreement with the conversion of the surface of Ga_2O_3 to TiO_2 and the spontaneous etching of the TiO_2 layer by HF. This mechanism could be confirmed by additional studies using vibrational spectroscopy or mass spectrometry.

Additional experiments explored the ability of HF and Tris(dimethylamido)gallium (TDMAG) to etch Ga_2O_3 films. TDMAG is the same metal precursor used for the growth of the Ga_2O_3 ALD film. TDMAG can be used as a metal precursor for ALE because TDMAG can provide dialkylamide ligands for ligand-exchange reactions. However, TDMAG cannot perform a conversion reaction because Ga_2O_3 and TDMAG both contain Ga.

Figure 11a shows the mass change versus reaction time during 20 Ga_2O_3 ALE cycles using HF and TDMAG exposures with a reaction sequence of 1-30-2-30. The sequential HF and TDMAG exposures linearly remove the Ga_2O_3 film. The mass change versus number of Ga_2O_3 ALE cycles yields a mass change per cycle of MCPC = −11.2 ng/(cm^2 cycle). This MCPC corresponds to an etch rate of 0.23 Å/cycle.

Figure 11b shows an enlargement of the mass changes versus time for three sequential HF and TDMAG exposures during Ga_2O_3 ALE in the steady-state, linear etching regime shown in Figure 11a. The mass changes are very different than the mass changes observed for HF with DMAC, TMA, or $TiCl_4$. The biggest distinction is that the TDMAG exposure produces an initial mass increase. This mass increase is followed by a slow mass loss. The total mass change during the TDMAG exposure prior to the subsequent HF exposure is ΔM_{TDMAG} = −4.8 ng/(cm^2 cycle).

The mass increase followed by the slow mass loss suggests that TDMAG initially adsorbs on the surface. Subsequently, the TDMAG undergoes a gradual ligand-exchange reaction with GaF_3 that leads to a progressive mass loss. The HF exposure does not cause a distinct mass change that coincides with the HF exposure. However, a progressive mass loss is observed and the mass loss after the HF exposure prior to the subsequent TDMAG exposure is ΔM_{HF} = −6.4 ng/(cm^2 cycle). The mass change from the HF exposure may be attributed to the combination between the mass loss expected from F replacement of $N(CH_3)_2$ and the mass gain expected from fluorination of the underlying Ga_2O_3 substrate.

3.3. Ex Situ Measurements of Ga_2O_3 ALE. Ex situ SE and XRR measurements were also performed to monitor Ga_2O_3 etching and to complement the in situ QCM measurements. Figure 12 shows the ex situ SE and XRR

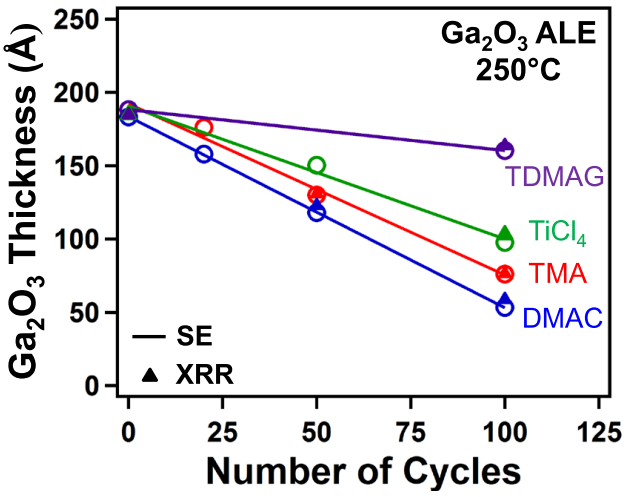

Figure 12. Film thickness versus number of cycles during Ga_2O_3 ALE with HF and TDMAG, $TiCl_4$, TMA, or DMAC as the metal precursor on Ga_2O_3 films on Si(100) at 250 °C determined by ex situ SE and XRR measurements.

studies using HF together with DMAC, TMA, $TiCl_4$, and TDMAB as the metal precursors at 250 °C. The etch rates were 1.3, 1.1, 0.91, and 0.28 Å/cycle with DMAC, TMA, $TiCl_4$, and TDMAB, respectively. These SE and XRR measurements are in good agreement with the QCM measurements. A summary of all of the Ga_2O_3 etch rates at

https://dx.doi.org/10.1021/acs.chemmater.0c00131
Chem. Mater. 2020, 32, 5937−5948

250 °C measured with the QCM, SE, and XRR techniques is given in Table 1.

Table 1. Summary of Ga_2O_3 Etch Rates at 250 °C Measured with QCM, SE, and XRR Techniques

	etch rate (Å/cycle) at 250 °C		
metal precursor	QCM	SE	XRR
TMA	0.82	1.1	1.1
$TiCl_4$	0.85	0.91	0.82
TDMAG	0.23	0.28	0.21
DMAC	1.2	1.3	1.3

XPS measurements were also used to survey the surface composition of the Ga_2O_3 films after the ALE reactions. These XPS measurements can help to identify the possible conversion-etch mechanism for Ga_2O_3 ALE. The XPS measurements observed noticeable levels of Al on the Ga_2O_3 surface after ALE with both TMA and DMAC. After Ga_2O_3 ALE using HF and TMA ending with the HF reaction, the films had 16 atom % Al and 19 atom % F. After Ga_2O_3 ALE using HF and DMAC ending with the HF reaction, the films had 6 atom % Al and 13 atom % F. These high levels of Al atom % and F atom % are consistent with the conversion of Ga_2O_3 to Al_2O_3 during Ga_2O_3 ALE and a high coverage of AlF_x species remaining on the surface.

Together with the QCM measurements shown in Figures 7 and 9b, the XPS measurements argue that the mechanism for Ga_2O_3 ALE must include both conversion reactions and fluorination and ligand-exchange reactions. There are also high concentrations of F observed after Ga_2O_3 ALE with HF and either DMAC or TMA ending with the HF reaction. These high F concentrations support the formation of GaF_3 and AlF_3 during the HF exposure. These fluorides would then be partially removed by the subsequent ligand-exchange reaction with DMAC or TMA. The XPS measurements also confirmed that there was <1 atom % of Cl on the etched Ga_2O_3 surface after Ga_2O_3 ALE with HF and DMAC ending with the HF reaction.

The XPS measurements after Ga_2O_3 ALE with HF and $TiCl_4$ ending with the HF reaction also revealed Ti concentrations. The XPS analysis measured ~2 atom % of Ti. The presence of Ti is consistent with Ga_2O_3 conversion to TiO_2 during the $TiCl_4$ exposure. The lower levels of Ti after the HF and $TiCl_4$ exposures compared with the Al levels after the HF and TMA or DMAC exposures may reflect the ability of HF to remove TiO_2. Earlier experiments suggested that HF could easily remove TiO_2 after TiN conversion to TiO_2.[52] In comparison, the ligand-exchange reaction between TMA and AlF_3 does not remove all of the AlF_3 layer.[24]

The XPS measurements after Ga_2O_3 ALE with HF and $TiCl_4$ ending with the HF reaction monitored F concentrations of only 1 atom % F. These low F concentrations are consistent with HF removing TiO_2 and a low coverage of GaF_x or TiF_x species on the surface. The XPS measurements also confirmed that there was <1 atom % of Cl on the etched Ga_2O_3 surface after Ga_2O_3 ALE with HF and $TiCl_4$ ending with the HF reaction.

3.4. Other Materials for Conversion and Fluorination and Ligand-Exchange Reactions. Ga_2O_3 can be etched by HF together with a large number of metal precursors including BCl_3, $AlCl(CH_3)_2$, $Al(CH_3)_3$, $TiCl_4$, and $Ga(N(CH_3)_2)_3$. The effectiveness of thermal Ga_2O_3 ALE is attributed to the potential for Ga_2O_3 etching by both conversion reactions and ligand-exchange reactions. The conversion reactions are possible because Ga_2O_3 has a fairly low heat of formation compared with other oxides such as B_2O_3, Al_2O_3, and TiO_2. Consequently, there is a possibility that the B-, Al-, or Ti-containing metal precursors for thermal ALE can convert the surface of Ga_2O_3 to B_2O_3, Al_2O_3, or TiO_2, respectively. Following this conversion, new pathways are available for thermal ALE in addition to the fluorination and ligand-exchange mechanism.

The potential for conversion reactions can be determined by a comparison of the heats of formation for the various materials. The relative stability of various materials, such as metal oxides, can be determined using Ellingham diagrams.[64,65] Materials that have smaller negative ΔG° values will have the potential of converting to materials that have larger negative ΔG° values. Conversion to B_2O_3, Al_2O_3, and TiO_2 are often preferred because these materials all have fairly large negative ΔG° values.

The thermochemistry of conversion reaction for various metal oxides to B_2O_3, Al_2O_3, and TiO_2 using BCl_3, $TiCl_4$, and $Al(CH_3)_3$, respectively, has been discussed earlier.[31,33] Table 2 gives the standard free energy changes for conversion reactions for some selected metal oxides at 250 °C. Conversion reactions increase the likelihood of thermal ALE for these materials because B_2O_3, Al_2O_3, and TiO_2 all have established pathways for thermal ALE.[4,20,24,33,52] Conversion reactions are particularly valuable for thermal ALE when fluorination would lead to the spontaneous etching of the material by producing a volatile fluoride.

Table 2. Thermochemistry of Conversion Reactions for Selected Metal Oxides Using BCl_3, $TiCl_4$, and $Al(CH_3)_3$ as the Metal Precursors[a]

BCl_3 conversion reactions	ΔG° (kcal)
$Ta_2O_5 + 10/3BCl_3(g) \rightarrow 5/3\ B_2O_3 + 2TaCl_5(g)$	−38.2
$1.5VO_2 + 2BCl_3(g) \rightarrow B_2O_3 + 1.5VCl_4(g)$	−37.1
$WO_3 + BCl_3(g) \rightarrow B_2O_3 + WCl_6(g)$	−5.6
$Nb_2O_5 + 10/3BCl_3(g) \rightarrow 5/3B_2O_3 + 2NbCl_5(g)$	−42.9
$TiCl_4$ conversion reactions	ΔG° (kcal)
$GeO_2 + TiCl_4(g) \rightarrow TiO_2 + GeCl_4(g)$	−24.9
$SnO_2 + TiCl_4(g) \rightarrow TiO_2 + SnCl_4(g)$	−21.4
$2MoO_3 + TiCl_4(g) \rightarrow TiO_2 + 2MoO_2Cl_2(g)$	−16.7
$Fe_2O_3 + 3/2TiCl_4(g) \rightarrow 3/2\ TiO_2 + 2FeCl_3(g)$	−6.0
$Al(CH_3)_3$ conversion reactions	ΔG° (kcal)
$3ZnO + 2Al(CH_3)_3(g) \rightarrow Al_2O_3 + 3Zn(CH_3)_2(g)$	−166.3
$1.5SiO_2 + 2Al(CH_3)_3(g) \rightarrow Al_2O_3 + 1.5Si(CH_3)_4(g)$	−198.5
$1.5SnO_2 + 2Al(CH_3)_3(g) \rightarrow Al_2O_3 + 1.5Sn(CH_3)_2(g)$	−228.1
$In_2O_3 + 2Al(CH_3)_3(g) \rightarrow Al_2O_3 + 2In(CH_3)_3(g)$	−317.9

[a]Standard free energy changes are given at 250 °C.[51]

4. CONCLUSIONS

Thermal Ga_2O_3 ALE was studied using HF and many different metal precursors including BCl_3, $AlCl(CH_3)_2$, $Al(CH_3)_3$, $TiCl_4$, and $Ga(N(CH_3)_2)_3$. In situ spectroscopic ellipsometry (SE) and quartz crystal microbalance (QCM) studies demonstrated that thermal Ga_2O_3 ALE was achieved using all of these metal precursors. The ease of etching Ga_2O_3 was attributed to the multiple pathways accessible for thermal Ga_2O_3 ALE. HF exposures can fluorinate the surface of Ga_2O_3

https://dx.doi.org/10.1021/acs.chemmater.0c00131
Chem. Mater. 2020, 32, 5937−5948

and produce GaF_3. Ligand-exchange reactions can then remove volatile Ga-containing products from the GaF_3 layer. Alternatively, the surface of Ga_2O_3 can be converted to a B_2O_3, Al_2O_3, or TiO_2 layer by the B-, Al-, or Ti-containing metal precursors. The B_2O_3 and TiO_2 layers can be spontaneously removed by HF exposures. The Al_2O_3 layer can be fluorinated and then removed by ligand-exchange reactions.

Using sequential exposures of HF and BCl_3, Ga_2O_3 etch rates varied from 0.59 to 1.35 Å/cycle at temperatures from 150 to 200 °C, respectively. A fluorination and ligand-exchange mechanism was proposed for thermal Ga_2O_3 ALE using HF and BCl_3 because the etching results did not depend on BCl_3 pressure. Ga_2O_3 could also be etched using HF and various other metal precursors. Ga_2O_3 etch rates at 250 °C were 1.2, 0.82, 0.85, and 0.23 Å/cycle for $AlCl(CH_3)_2$, $Al(CH_3)_3$, $TiCl_4$, and $Ga(N(CH_3)_2)_3$ as the metal precursors, respectively. The mass changes during QCM measurements of thermal Ga_2O_3 ALE using HF together with $AlCl(CH_3)_2$ and $Al(CH_3)_3$ were consistent with a fluorination and ligand-exchange mechanism. XPS measurements also showed that the $AlCl(CH_3)_2$ and $Al(CH_3)_3$ exposures lead to the conversion of Ga_2O_3 to Al_2O_3.

Distinctly different mass changes were observed during QCM measurements of thermal Ga_2O_3 ALE using HF and $TiCl_4$. These mass changes were consistent with the conversion of the surface of Ga_2O_3 to TiO_2 and then the spontaneous removal of the TiO_2 layer by HF. XPS measurements observed Ti signal intensities that were consistent with Ga_2O_3 conversion to TiO_2 during the $TiCl_4$ exposures. Thermal Ga_2O_3 ALE using HF and $Ga(N(CH_3)_2)_3$ exposures also displayed different mass changes that suggested that $Ga(N(CH_3)_2)_3$ can adsorb on the fluorinated Ga_2O_3 surface prior to the ligand-exchange reaction.

The ability of various metal precursors to either convert Ga_2O_3 or to undergo ligand-exchange reactions with the fluorinated surface layer leads to multiple pathways for efficient thermal Ga_2O_3 ALE. These different pathways will be useful to develop selectivity in ALE between Ga_2O_3 and other materials. Ga_2O_3 can be etched using BCl_3, $AlCl(CH_3)_2$, $Al(CH_3)_3$, $TiCl_4$, and $Ga(N(CH_3)_2)_3$ as metal precursors. Other materials may be etched by none or only some of these metal precursors. Knowledge of which metal precursors will etch various materials builds a portfolio that will enable selective thermal ALE during device fabrication.

AUTHOR INFORMATION

Corresponding Author

Steven M. George − *Department of Chemistry, University of Colorado, Boulder, Colorado 80309, United States;* orcid.org/0000-0003-0253-9184; Email: steven.george@colorado.edu

Authors

Younghee Lee − *Department of Chemistry, University of Colorado, Boulder, Colorado 80309, United States;* orcid.org/0000-0002-0492-6826

Nicholas R. Johnson − *Department of Chemistry, University of Colorado, Boulder, Colorado 80309, United States*

Complete contact information is available at: https://pubs.acs.org/10.1021/acs.chemmater.0c00131

Notes

The authors declare no competing financial interest.

ACKNOWLEDGMENTS

This research was funded by the Semiconductor Research Corporation (SRC) and by the Intel Corporation through the SRC. The authors thank Andrew S. Cavanagh for the XPS analysis. The authors also thank Advanced Energy for equipment used to assemble the inductively coupled plasma (ICP) source.

REFERENCES

(1) Carver, C. T.; Plombon, J. J.; Romero, P. E.; Suri, S.; Tronic, T. A.; Turkot, R. B. Atomic Layer Etching: An Industry Perspective. *ECS J. Solid State Sci. Technol.* **2015**, *4*, N5005−N5009.

(2) Kanarik, K. J.; Lill, T.; Hudson, E. A.; Sriraman, S.; Tan, S.; Marks, J.; Vahedi, V.; Gottscho, R. A. Overview of Atomic Layer Etching in the Semiconductor Industry. *J. Vac. Sci. Technol., A* **2015**, *33*, No. 020802.

(3) George, S. M.; Lee, Y. Prospects for Thermal Atomic Layer Etching Using Sequential, Self-Limiting Fluorination and Ligand-Exchange Reactions. *ACS Nano* **2016**, *10*, 4889−4894.

(4) Lee, Y.; George, S. M. Atomic Layer Etching of Al_2O_3 Using Sequential, Self-Limiting Thermal Reactions with $Sn(acac)_2$ and HF. *ACS Nano* **2015**, *9*, 2061−2070.

(5) Matsuura, T.; Murota, J.; Sawada, Y.; Ohmi, T. Self-Limited Layer-by-Layer Etching of Si by Alternated Chlorine Adsorption and Ar^+ Ion Irradiation. *Appl. Phys. Lett.* **1993**, *63*, 2803−2805.

(6) Park, S. D.; Min, K. S.; Yoon, B. Y.; Lee, D. H.; Yeom, G. Y. Precise Depth Control of Silicon Etching Using Chlorine Atomic Layer Etching. *Jpn. J. Appl. Phys.* **2005**, *44*, 389−393.

(7) Sakaue, H.; Iseda, S.; Asami, K.; Yamamoto, J.; Hirose, M.; Horiike, Y. Atomic Layer Controlled Digital Etching of Silicon. *Jpn. J. Appl. Phys.* **1990**, *29*, 2648−2652.

(8) Suzue, K.; Matsuura, T.; Murota, J.; Sawada, Y.; Ohmi, T. Substrate Orientation Dependence of Self-Limited Atomic Layer Etching of Si with Chlorine Adsorption and Low Energy Ar^+ Irradiation. *Appl. Surf. Sci.* **1994**, *82*−*83*, 422−427.

(9) Gasvoda, R. J.; van de Steeg, A. W.; Bhowmick, R.; Hudson, E. A.; Agarwal, S. Surface Phenomena During Plasma-Assisted Atomic Layer Etching of SiO_2. *ACS Appl. Mater. Interfaces* **2017**, *9*, 31067−31075.

(10) Metzler, D.; Bruce, R. L.; Engelmann, S.; Joseph, E. A.; Oehrlein, G. S. Fluorocarbon Assisted Atomic Layer Etching of SiO_2 Using Cyclic Ar/C_4F_8 Plasma. *J. Vac. Sci. Technol., A* **2014**, *32*, No. 020603.

(11) Park, S. D.; Lim, W. S.; Park, B. J.; Lee, H. C.; Bae, J. W.; Yeom, G. Y. Precise Depth Control and Low Damage Atomic Layer Etching of HfO_2 using BCl_3 and Ar Neutral Beam. *Electrochem. Solid-State Lett.* **2008**, *11*, H71−H73.

(12) Min, K. S.; Kang, S. H.; Kim, J. K.; Jhon, Y. I.; Jhon, M. S.; Yeom, G. Y. Atomic Layer Etching of Al_2O_3 Using BCl_3/Ar for the Interface Passivation Layer of III-V MOS Devices. *Microelectron. Eng.* **2013**, *110*, 457−460.

(13) Park, S. D.; Oh, C. K.; Bae, J. W.; Yeom, G. Y.; Kim, T. W.; Song, J. I.; Jang, J. H. Atomic Layer Etching of InP Using a Low Angle Forward Reflected Ne Neutral Beam. *Appl. Phys. Lett.* **2006**, *89*, No. 043109.

(14) Kauppinen, C.; Khan, S. A.; Sundqvist, J.; Suyatin, D. B.; Suihkonen, S.; Kauppinen, E. I.; Sopanen, M. Atomic Layer Etching of Gallium Nitride (0001). *J. Vac. Sci. Technol., A* **2017**, *35*, No. 060603.

(15) Kim, D. S.; Kim, J. E.; Lee, W. O.; Park, J. W.; Gill, Y. J.; Jeong, B. H.; Yeom, G. Y. Anisotropic Atomic Layer Etching of W Using Fluorine Radicals/Oxygen Ion Beam. *Plasma Processes Polym.* **2019**, *16*, No. e1900081.

(16) Lim, W. S.; Kim, Y. Y.; Kim, H.; Jang, S.; Kwon, N.; Park, B. J.; Ahn, J. H.; Chung, I.; Hong, B. H.; Yeom, G. Y. Atomic Layer Etching of Graphene for Full Graphene Device Fabrication. *Carbon* **2012**, *50*, 429−435.

(17) Vogli, E.; Metzler, D.; Oehrlein, G. S. Feasibility of Atomic Layer Etching of Polymer Material Based on Sequential O_2 Exposure

and Ar Low-Pressure Plasma-Etching. *Appl. Phys. Lett.* **2013**, *102*, No. 253105.
(18) Zywotko, D. R.; Faguet, J.; George, S. M. Rapid Atomic Layer Etching of Al_2O_3 Using Sequential Exposures of Hydrogen Fluoride and Trimethylaluminum with No Purging. *J. Vac. Sci. Technol., A* **2018**, *36*, No. 061508.
(19) Fischer, A.; Routzahn, A.; Lee, Y.; Lill, T.; George, S. M. Thermal Etching of AlF_3 and Thermal Atomic Layer Etching of Al_2O_3. *J. Vac. Sci. Technol., A* **2020**, *38*, No. 022603.
(20) Lee, Y.; George, S. M. Thermal Atomic Layer Etching of Al_2O_3, HfO_2, and ZrO_2 Using Sequential Hydrogen Fluoride and Dimethylaluminum Chloride Exposures. *J. Phys. Chem. C* **2019**, *123*, 18455−18466.
(21) George, S. M. Mechanisms of Thermal Atomic Layer Etching. *Acc. Chem. Res.* **2020**, *53*, 1151−1160.
(22) Gertsch, J. C.; Cano, A. M.; Bright, V. M.; George, S. M. SF_4 as the Fluorination Reactant for Al_2O_3 and VO_2 Thermal Atomic Layer Etching. *Chem. Mater.* **2019**, *31*, 3624−3635.
(23) Lee, Y.; DuMont, J. W.; George, S. M. Mechanism of Thermal Al_2O_3 Atomic Layer Etching Using Sequential Reactions with $Sn(acac)_2$ and HF. *Chem. Mater.* **2015**, *27*, 3648−3657.
(24) Lee, Y.; DuMont, J. W.; George, S. M. Trimethylaluminum as the Metal Precursor for the Atomic Layer Etching of Al_2O_3 Using Sequential, Self-Limiting Thermal Reactions. *Chem. Mater.* **2016**, *28*, 2994−3003.
(25) Lee, Y.; Huffman, C.; George, S. M. Selectivity in Thermal Atomic Layer Etching Using Sequential, Self-Limiting Fluorination and Ligand-Exchange Reactions. *Chem. Mater.* **2016**, *28*, 7657−7665.
(26) Cano, A. M.; Marquardt, A. E.; DuMont, J. W.; George, S. M. Effect of HF Pressure on Thermal Al_2O_3 Atomic Layer Etch Rates and Al_2O_3 Fluorination. *J. Phys. Chem. C* **2019**, *123*, 10346−10355.
(27) Hennessy, J.; Moore, C. S.; Balasubramanian, K.; Jewell, A. D.; France, K.; Nikzad, S. Enhanced Atomic Layer Etching of Native Aluminum Oxide for Ultraviolet Optical Applications. *J. Vac. Sci. Technol., A* **2017**, *35*, No. 041512.
(28) Lee, Y.; George, S. M. Thermal Atomic Layer Etching of HfO_2 Using HF for Fluorination and $TiCl_4$ for Ligand-Exchange. *J. Vac. Sci. Technol., A* **2018**, *36*, No. 061504.
(29) Johnson, N. R.; Sun, H. X.; Sharma, K.; George, S. M. Thermal Atomic Layer Etching of Crystalline Aluminum Nitride Using Sequential, Self-limiting Hydrogen Fluoride and $Sn(acac)_2$ Reactions and Enhancement by H_2 and Ar Plasmas. *J. Vac. Sci. Technol., A* **2016**, *34*, No. 050603.
(30) Johnson, N. R.; Hite, J. K.; Mastro, M. A.; Eddy, C. R.; George, S. M. Thermal Atomic Layer Etching of Crystalline GaN Using Sequential Exposures of XeF_2 and BCl_3. *Appl. Phys. Lett.* **2019**, *114*, No. 243103.
(31) Zywotko, D. R.; George, S. M. Thermal Atomic Layer Etching of ZnO by a "Conversion-Etch" Mechanism Using Sequential Exposures of Hydrogen Fluoride and Trimethylaluminum. *Chem. Mater.* **2017**, *29*, 1183−1191.
(32) DuMont, J. W.; Marquardt, A. E.; Cano, A. M.; George, S. M. Thermal Atomic Layer Etching of SiO_2 by a "Conversion-Etch" Mechanism Using Sequential Reactions of Trimethylaluminum and Hydrogen Fluoride. *ACS Appl. Mater. Interfaces* **2017**, *9*, 10296−10307.
(33) Johnson, N. R.; George, S. M. WO_3 and W Thermal Atomic Layer Etching Using "Conversion-Fluorination" and "Oxidation-Conversion-Fluorination" Mechanisms. *ACS Appl. Mater. Interfaces* **2017**, *9*, 34435−34447.
(34) Abdulagatov, A. I.; George, S. M. Thermal Atomic Layer Etching of Silicon Using O_2, HF, and $Al(CH_3)_3$ as the Reactants. *Chem. Mater.* **2018**, *30*, 8465−8475.
(35) Abdulagatov, A. I.; George, S. M. Thermal Atomic Layer Etching of Silicon Nitride Using an Oxidation and "Conversion Etch" Mechanism. *J. Vac. Sci. Technol., A* **2020**, *38*, No. 022607.
(36) Galazka, Z. beta-Ga_2O_3 for Wide-Bandgap Electronics and Optoelectronics. *Semicond. Sci. Technol.* **2018**, *33*, No. 113001.
(37) Higashiwaki, M.; Jessen, G. H. Guest Editorial: The Dawn of Gallium Oxide Microelectronics. *Appl. Phys. Lett.* **2018**, *112*, No. 060401.
(38) Higashiwaki, M.; Sasaki, K.; Murakami, H.; Kumagai, Y.; Koukitu, A.; Kuramata, A.; Masui, T.; Yamakoshi, S. Recent Progress in Ga_2O_3 Power Devices. *Semicond. Sci. Technol.* **2016**, *31*, No. 034001.
(39) Pearton, S. J.; Yang, J. C.; Cary, P. H.; Ren, F.; Kim, J.; Tadjer, M. J.; Mastro, M. A. A Review of Ga_2O_3 Materials, Processing, and Devices. *Appl. Phys. Rev.* **2018**, *5*, No. 011301.
(40) Stepanov, S. I.; Nikolaev, V. I.; Bougrov, V. E.; Romanov, A. E. Gallium Oxide: Properties and Applications - A Review. *Rev. Adv. Mater. Sci.* **2016**, *44*, 63−86.
(41) Zhang, Y. W.; Neal, A.; Xia, Z. B.; Joishi, C.; Johnson, J. M.; Zheng, Y. H.; Bajaj, S.; Brenner, M.; Dorsey, D.; Chabak, K.; Jessen, G.; Hwang, J.; Mou, S.; Heremans, J. P.; Rajan, S. Demonstration of High Mobility and Quantum Transport in Modulation-Doped beta-$(Al_xGa_{1-x})_2O_3/Ga_2O_3$ Heterostructures. *Appl. Phys. Lett.* **2018**, *112*, No. 173502.
(42) Higashiwaki, M.; Sasaki, K.; Kuramata, A.; Masui, T.; Yamakoshi, S. Gallium oxide (Ga_2O_3) Metal-Semiconductor Field-Effect Transistors on Single-Crystal beta-Ga_2O_3 (010) Substrates. *Appl. Phys. Lett.* **2012**, *100*, No. 013504.
(43) Ghosh, K.; Singisetti, U. Ab Initio Velocity-Field Curves in Monoclinic beta-Ga_2O_3. *J. Appl. Phys.* **2017**, *122*, No. 035702.
(44) Canali, C.; Ottaviani, G. Saturation Values of Electron Drift Velocity in Silicon between 300 Degrees K and 4.2 Degrees K. *Phys. Lett. A* **1970**, *32*, 147−148.
(45) Sasaki, K.; Thieu, Q. T.; Wakimoto, D.; Koishikawa, Y.; Kuramata, A.; Yamakoshi, S. Depletion-Mode Vertical Ga_2O_3 Trench MOSFETs Fabricated Using Ga_2O_3 Homoepitaxial Films Grown by Halide Vapor Phase Epitaxy. *Appl. Phys. Express* **2017**, *10*, No. 124201.
(46) Chabak, K. D.; Moser, N.; Green, A. J.; Walker, D. E.; Tetlak, S. E.; Heller, E.; Crespo, A.; Fitch, R.; McCandless, J. P.; Leedy, K.; Baldini, M.; Wagner, G.; Galazka, Z.; Li, X. L.; Jessen, G. Enhancement-Mode Ga_2O_3 Wrap-Gate Fin Field-Effect Transistors on Native (100) beta-Ga_2O_3 Substrate with High Breakdown Voltage. *Appl. Phys. Lett.* **2016**, *109*, No. 213501.
(47) Higashiwaki, M.; Sasaki, K.; Kamimura, T.; Wong, M. H.; Krishnamurthy, D.; Kuramata, A.; Masui, T.; Yamakoshi, S. Depletion-Mode Ga_2O_3 Metal-Oxide-Semiconductor Field-Effect Transistors on beta-Ga_2O_3 (010) Substrates and Temperature Dependence of their Device Characteristics. *Appl. Phys. Lett.* **2013**, *103*, No. 123511.
(48) Shih, H. Y.; Chu, F. C.; Das, A.; Lee, C. Y.; Chen, M. J.; Lin, R. M. Atomic Layer Deposition of Gallium Oxide Films as Gate Dielectrics in AlGaN/GaN Metal-Oxide-Semiconductor High-Electron-Mobility Transistors. *Nanoscale Res. Lett.* **2016**, *11*, 1−9.
(49) Hogan, J. E.; Kaun, S. W.; Ahmadi, E.; Oshima, Y.; Speck, J. S. Chlorine-Based Dry Etching of beta-Ga_2O_3. *Semicond. Sci. Technol.* **2016**, *31*, No. 065006.
(50) Okumura, H.; Tanaka, T. Dry and Wet Etching for beta-Ga_2O_3 Schottky Barrier Diodes with Mesa Termination. *Jpn. J. Appl. Phys.* **2019**, *58*, No. 120902.
(51) *HSC Chemistry*, version 5.1; Outokumpu Research Oy: Pori, Finland, 2002.
(52) Lee, Y.; George, S. M. Thermal Atomic Layer Etching of Titanium Nitride Using Sequential, Self-Limiting Reactions: Oxidation to TiO_2 and Fluorination to Volatile TiF_4. *Chem. Mater.* **2017**, *29*, 8202−8210.
(53) Kondati Natarajan, S.; Elliott, S. D. Modeling the Chemical Mechanism of the Thermal Atomic Layer Etch of Aluminum Oxide: A Density Functional Theory Study of Reactions during HF Exposure. *Chem. Mater.* **2018**, *30*, 5912−5922.
(54) Clancey, J. W.; Cavanagh, A. S.; Smith, J. E. T.; Sharma, S.; George, S. M. Volatile Etch Species Produced During Thermal Al_2O_3 Atomic Layer Etching. *J. Phys. Chem. C* **2020**, *124*, 287−299.

https://dx.doi.org/10.1021/acs.chemmater.0c00131
Chem. Mater. 2020, 32, 5937−5948

(55) Donmez, I.; Ozgit-Akgun, C.; Biyikli, N. Low Temperature Deposition of Ga_2O_3 Thin Films Using Trimethylgallium and Oxygen Plasma. *J. Vac. Sci. Technol., A* **2013**, *31*, No. 01A110.
(56) Clancey, J. W.; Cavanagh, A. S.; Kukreja, R. S.; Kongkanand, A.; George, S. M. Atomic Layer Deposition of Ultrathin Platinum Films on Tungsten Atomic Layer Deposition Adhesion Layers: Application to High Surface Area Substrates. *J. Vac. Sci. Technol., A* **2015**, *33*, No. 01A130.
(57) Lee, Y.; DuMont, J. W.; George, S. M. Atomic Layer Etching of HfO_2 Using Sequential, Self-Limiting Thermal Reactions with $Sn(acac)_2$ and HF. *ESC J. Solid State Sci. Technol.* **2015**, *4*, N5013−N5022.
(58) Elam, J. W.; Groner, M. D.; George, S. M. Viscous Flow Reactor with Quartz Crystal Microbalance for Thin Film Growth by Atomic Layer Deposition. *Rev. Sci. Instrum.* **2002**, *73*, 2981−2987.
(59) Dezelah, C. L.; Niinisto, J.; Arstila, K.; Niinisto, L.; Winter, C. H. Atomic Layer Deposition of Ga_2O_3 Films From a Dialkylamido-Based Precursor. *Chem. Mater.* **2006**, *18*, 471−475.
(60) Lee, Y.; DuMont, J. W.; Cavanagh, A. S.; George, S. M. Atomic Layer Deposition of AlF_3 Using Trimethylaluminum and Hydrogen Fluoride. *J. Phys. Chem. C* **2015**, *119*, 14185−14194.
(61) Lee, Y.; Sun, H. X.; Young, M. J.; George, S. M. Atomic Layer Deposition of Metal Fluorides Using HF-Pyridine as the Fluorine Precursor. *Chem. Mater.* **2016**, *28*, 2022−2032.
(62) Rebien, M.; Henrion, W.; Hong, M.; Mannaerts, J. P.; Fleischer, M. Optical Properties of Gallium Oxide Thin Films. *Appl. Phys. Lett.* **2002**, *81*, 250−252.
(63) Deal, B. E.; Grove, A. S. General Relationship for Thermal Oxidation of Silicon. *J. Appl. Phys.* **1965**, *36*, 3770−3778.
(64) Sato, S.; Honjo, H.; Ikeda, S.; Ohno, H.; Endoh, T.; Niwa, M. Evidence of a Reduction Reaction of Oxidized Iron/Cobalt by Boron Atoms Diffused Toward Naturally Oxidized Surface of CoFeB Layer During Annealing. *Appl. Phys. Lett.* **2015**, *106*, No. 142407.
(65) Ellingham, H. J. T. Reducibility of Oxides and Sulphides in Metallurgical Processes. *J. Soc. Chem. Ind., London* **1944**, *63*, 125−133.

https://dx.doi.org/10.1021/acs.chemmater.0c00131
Chem. Mater. 2020, 32, 5937−5948